Lechner et al. Supplemental Fig. 1

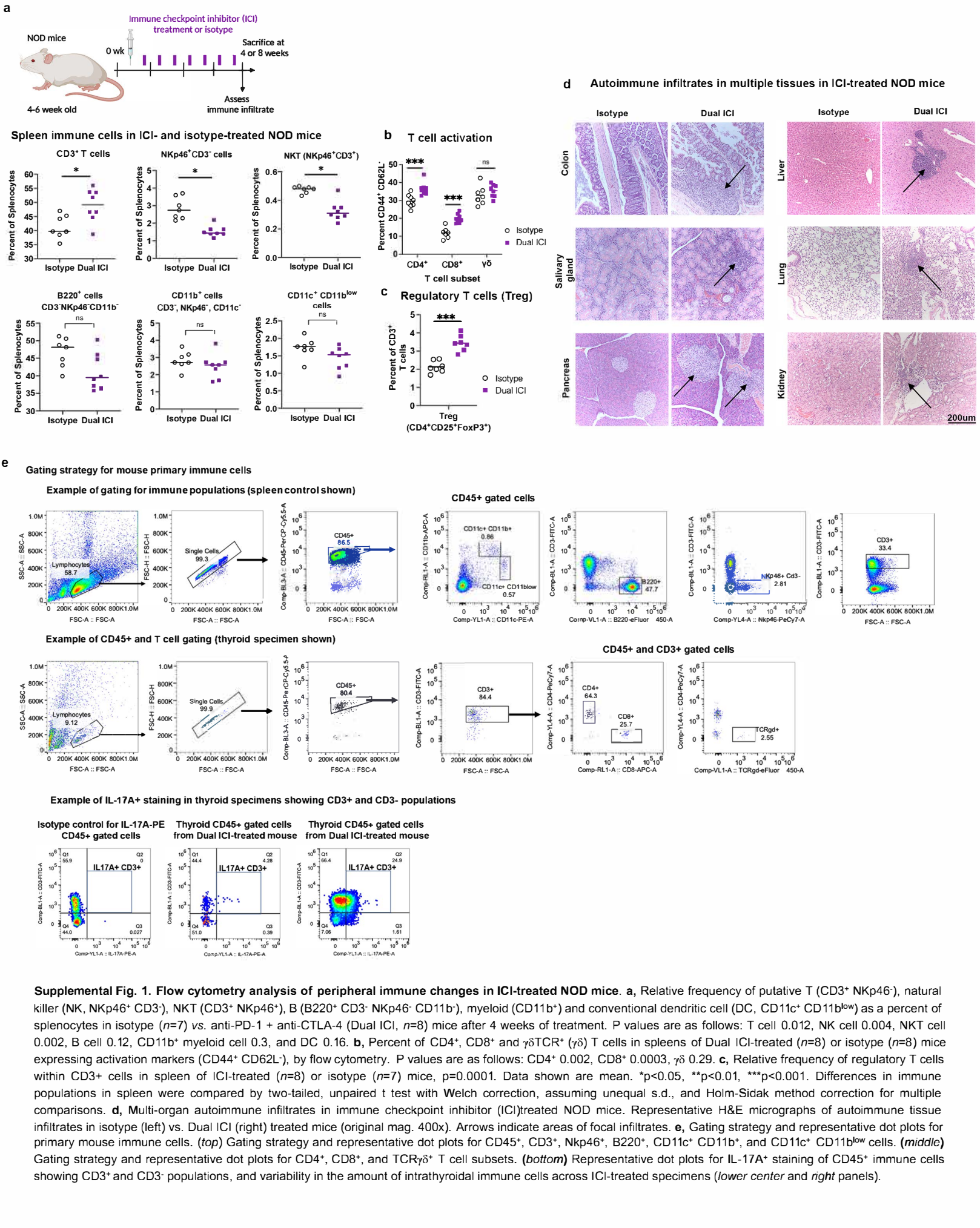

Supplemental Fig. 1. Flow cytometry analysis of peripheral immune changes in ICI-treated NOD mice. **a,** Relative frequency of putative T ($CD3^+$ $NKp46^-$), natural killer (NK, $NKp46^+$ $CD3^-$), NKT ($CD3^+$ $NKp46^+$), B ($B220^+$ $CD3^-$ $NKp46^-$ $CD11b^-$), myeloid ($CD11b^+$) and conventional dendritic cell (DC, $CD11c^+$ $CD11b^{low}$) as a percent of splenocytes in isotype (*n*=7) *vs.* anti-PD-1 + anti-CTLA-4 (Dual ICI, *n*=8) mice after 4 weeks of treatment. P values are as follows: T cell 0.012, NK cell 0.004, NKT cell 0.002, B cell 0.12, $CD11b^+$ myeloid cell 0.3, and DC 0.16. **b,** Percent of $CD4^+$, $CD8^+$ and $\gamma\delta TCR^+$ ($\gamma\delta$) T cells in spleens of Dual ICI-treated (*n*=8) or isotype (*n*=8) mice expressing activation markers ($CD44^+$ $CD62L^-$), by flow cytometry. P values are as follows: $CD4^+$ 0.002, $CD8^+$ 0.0003, $\gamma\delta$ 0.29. **c,** Relative frequency of regulatory T cells within CD3+ cells in spleen of ICI-treated (*n*=8) or isotype (*n*=7) mice, p=0.0001. Data shown are mean. *p<0.05, **p<0.01, ***p<0.001. Differences in immune populations in spleen were compared by two-tailed, unpaired t test with Welch correction, assuming unequal s.d., and Holm-Sidak method correction for multiple comparisons. **d,** Multi-organ autoimmune infiltrates in immune checkpoint inhibitor (ICI)treated NOD mice. Representative H&E micrographs of autoimmune tissue infiltrates in isotype (left) vs. Dual ICI (right) treated mice (original mag. 400x). Arrows indicate areas of focal infiltrates. **e,** Gating strategy and representative dot plots for primary mouse immune cells. (*top*) Gating strategy and representative dot plots for $CD45^+$, $CD3^+$, $Nkp46^+$, $B220^+$, $CD11c^+$ $CD11b^+$, and $CD11c^+$ $CD11b^{low}$ cells. **(*middle*)** Gating strategy and representative dot plots for $CD4^+$, $CD8^+$, and $TCR\gamma\delta^+$ T cell subsets. **(*bottom*)** Representative dot plots for IL-$17A^+$ staining of $CD45^+$ immune cells showing $CD3^+$ and $CD3^-$ populations, and variability in the amount of intrathyroidal immune cells across ICI-treated specimens (*lower center* and *right* panels).

Lechner Supplemental Fig. 2

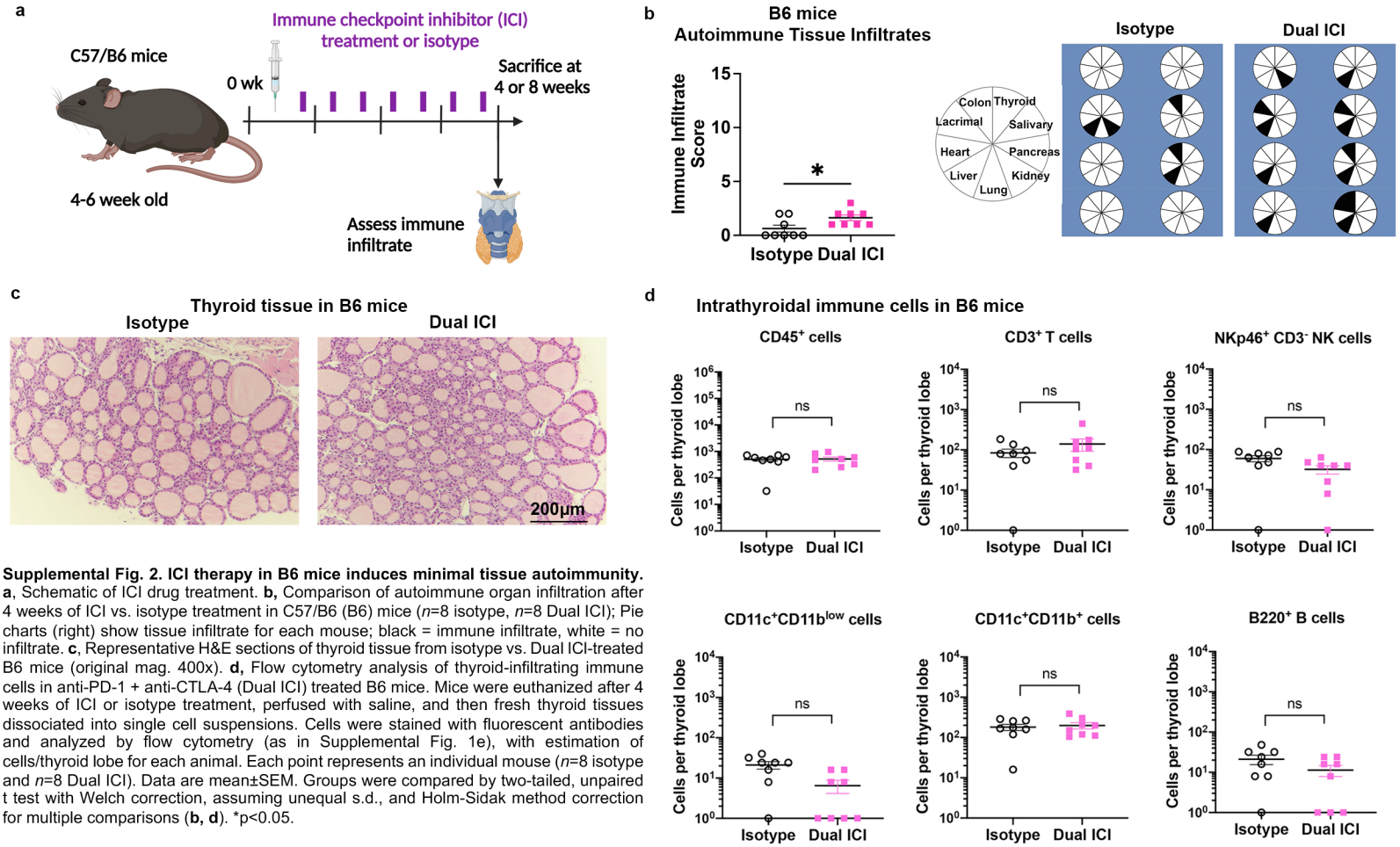

Supplemental Fig. 2. ICI therapy in B6 mice induces minimal tissue autoimmunity. **a**, Schematic of ICI drug treatment. **b,** Comparison of autoimmune organ infiltration after 4 weeks of ICI vs. isotype treatment in C57/B6 (B6) mice (*n*=8 isotype, *n*=8 Dual ICI); Pie charts (right) show tissue infiltrate for each mouse; black = immune infiltrate, white = no infiltrate. **c**, Representative H&E sections of thyroid tissue from isotype vs. Dual ICI-treated B6 mice (original mag. 400x). **d,** Flow cytometry analysis of thyroid-infiltrating immune cells in anti-PD-1 + anti-CTLA-4 (Dual ICI) treated B6 mice. Mice were euthanized after 4 weeks of ICI or isotype treatment, perfused with saline, and then fresh thyroid tissues dissociated into single cell suspensions. Cells were stained with fluorescent antibodies and analyzed by flow cytometry (as in Supplemental Fig. 1e), with estimation of cells/thyroid lobe for each animal. Each point represents an individual mouse (*n*=8 isotype and *n*=8 Dual ICI). Data are mean±SEM. Groups were compared by two-tailed, unpaired t test with Welch correction, assuming unequal s.d., and Holm-Sidak method correction for multiple comparisons (**b, d**). *p<0.05.

Lechner et al. Supplemental Fig. 3

a Gene expression across cell clusters in mouse intrathyroidal immune cells by scRNAseq

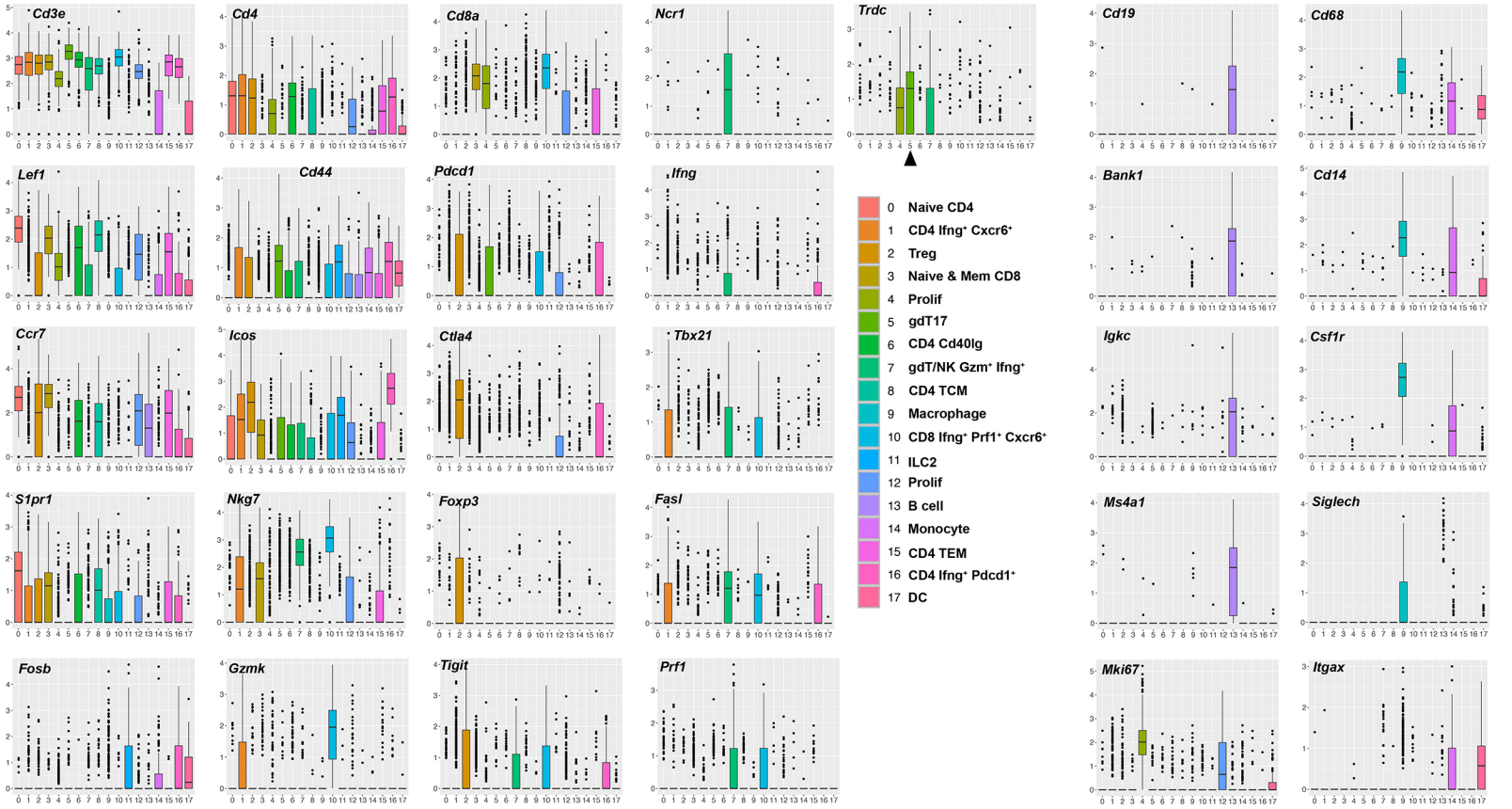

b

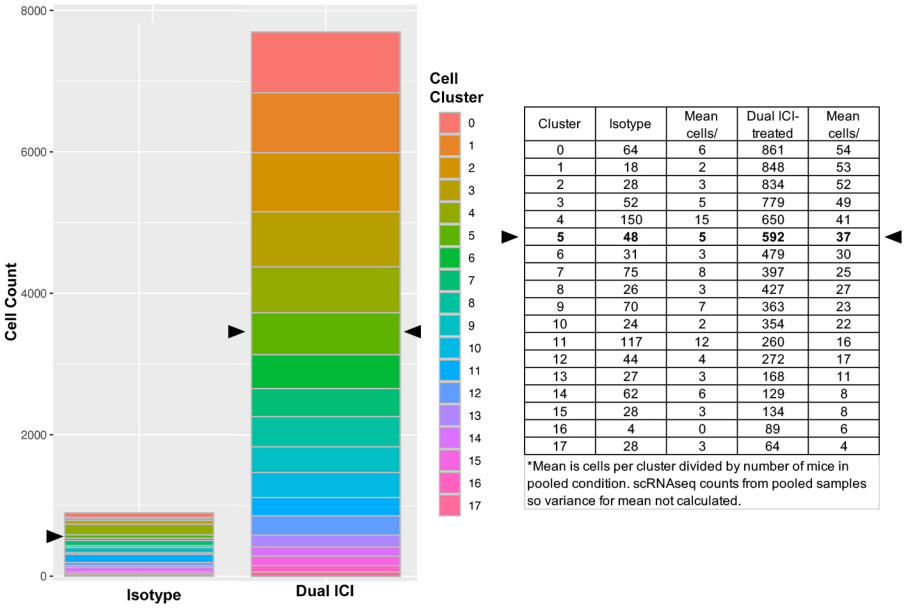

Cluster	Isotype	Mean cells/	Dual ICI-treated	Mean cells/
0	64	6	861	54
1	18	2	848	53
2	28	3	834	52
3	52	5	779	49
4	150	15	650	41
5	**48**	**5**	**592**	**37**
6	31	3	479	30
7	75	8	397	25
8	26	3	427	27
9	70	7	363	23
10	24	2	354	22
11	117	12	260	16
12	44	4	272	17
13	27	3	168	11
14	62	6	129	8
15	28	3	134	8
16	4	0	89	6
17	28	3	64	4

*Mean is cells per cluster divided by number of mice in pooled condition. scRNAseq counts from pooled samples so variance for mean not calculated.

c Type 3 immune response

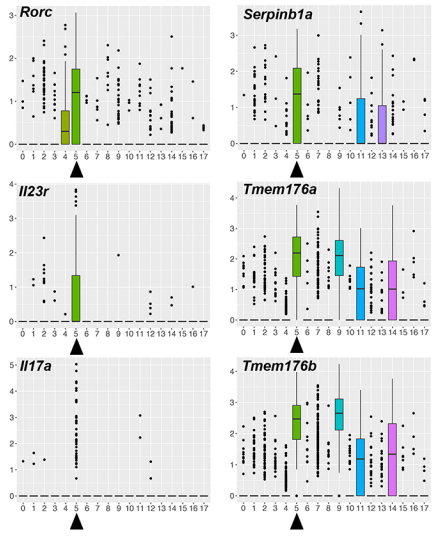

d IL-17A driven chemokines

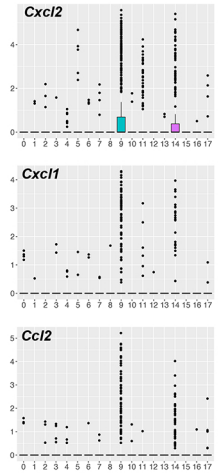

Supplemental Fig. 3. Supplemental data for scRNAseq of thyroid immune infiltrates from isotype or Dual !CI-treated NOD mice. a, The expression levels of various marker genes of each cluster in mouse thyroid tissue UMAP clusters for relevant immune populations. **b,** Stacked bar plot showing the composition by cell count for pooled thyroid specimens (n= 10 for isotype treated mice, n= 16 for ICI-treated mice) in each condition for relevant immune populations (left). Cell counts for each cluster for pooled specimens and mean per mouse (total count divide by mouse number) (right). Variance measure not calculated as data is from pooled specimens. **c,** Expression of immune genes associated with Type 3 immune responses across cell clusters. **d,** expression of myeloid cell recruiting IL-17A driven chemokines across cell clusters.

Lechner et al. Supplemental Fig. 4

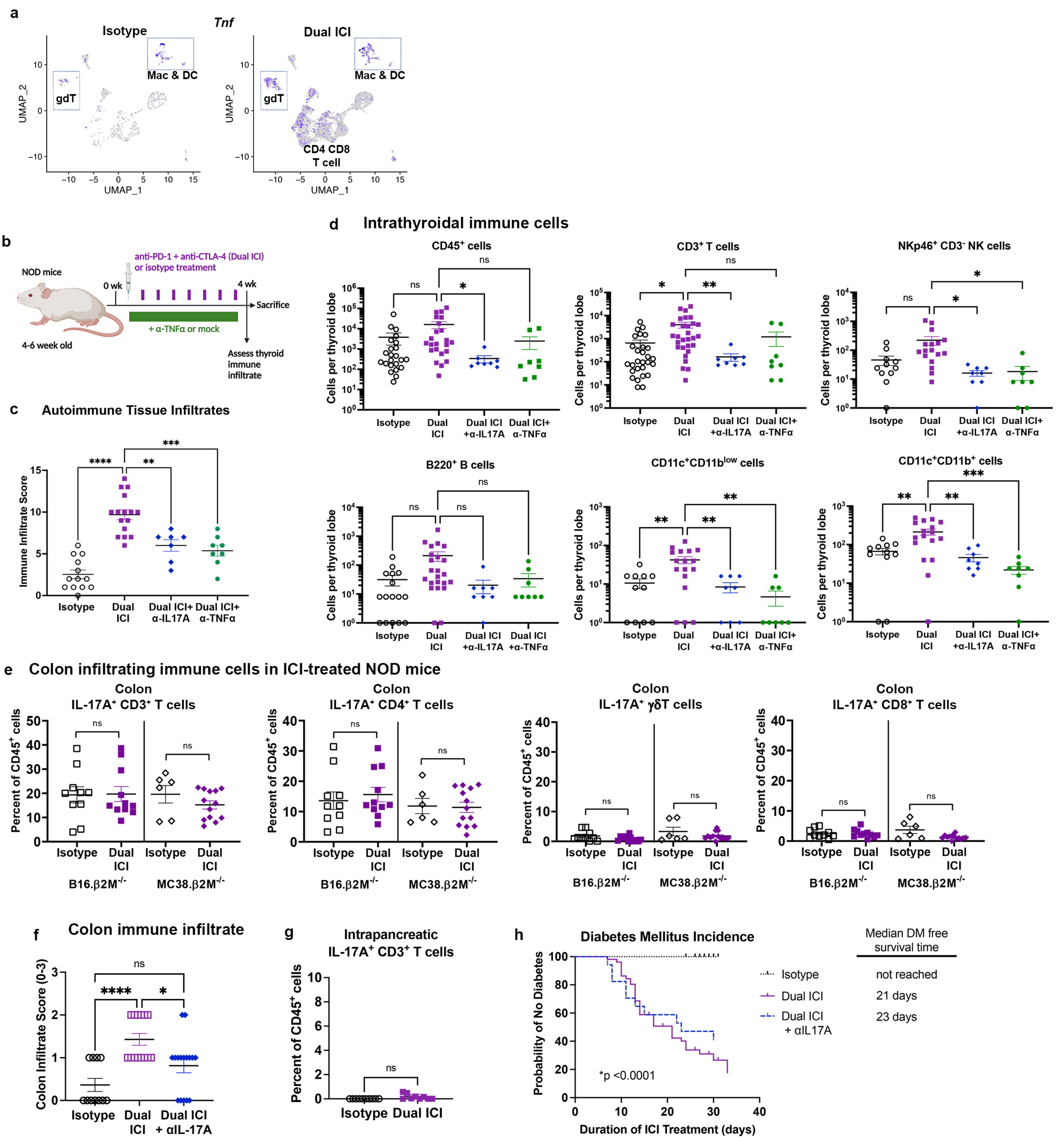

Supplemental Figure 4. Role of IL-17A axis cytokine TNFa in autoimmune thyroid infiltrates and IL-17A+ T cells in non-thyroid tissues of ICI-treated mice. a, Feature plot showing expression of *Tnf* by thyroid infiltrating immune cells in isotype or Dual ICI-treated NOD mice by scRNAseq. **b,** Schematic of treatment regimen. **c**, Autoimmune organ infiltrate score after 4 weeks of ICI treatment in isotype (*n*=14), Dual ICI (*n*=16), Dual ICI + neutralizing IL-17A antibody (αIL17A, *n*=7), and Dual ICI + neutralizing TNFα antibody (αTNFα, *n*=8). **d**, Intrathyroidal immune cell frequency among groups, Dual ICI, Dual ICI + αIL17A, Dual ICI + αTNFα. Each dot represents one animal. Data are mean ±SEM. In **c** and **d,** data from main **Figure 4** are reshown for comparison purposes with Dual ICI + αTNFα (data were derived from the same experiments). **e,** IL-17A$^+$ T cells in gut of ICI-treated NOD mice. Relative frequency among CD45$^+$ immune cells of IL-17A$^+$ CD3$^+$ T cells and IL-17A$^+$ T cell subsets isolated from colon tissue of isotype or Dual ICI-treated mice at 4 weeks by flow cytometry, 3 experiments, each dot represents a single animal. **f**, Comparison of colon immune infiltrate on histology for isotype (*n*=11), Dual ICI-treated (*n*=11), or Dual ICI and neutralizing IL-17A (αIL17A) therapy (*n*=14) NOD mice after 4 weeks, 2 experiments, each dot represents a single animal. **g**, Relative frequency among CD45$^+$ immune cells of IL-17A$^+$ T cells in the pancreas of isotype *vs.* Dual ICI-treated mice, 2 experiments, each dot represents a single animal. **h,** Kaplan-Meier curve showing incident autoimmune diabetes mellitus in NOD mice among treatment groups as assessed by persistent glucosuria requiring insulin therapy. Data are mean ±SEM shown. **p<0.01, ***p<0.001, ****p<0.0001. Brown-Forsythe ANOVA, assuming unequal s.d., followed by Dunnett's multiple comparisons test as indicated (**c-d**). Two-tailed, unpaired t test with Welch correction, assuming unequal s.d. and Holm-Sidak method correction for multiple comparisons (**e,g**); Log rank test for trend for median diabetes-free survival (**h**).